

Single-particle motion at large distances in $2N+core$ cluster systems near the drip line: a challenge for nuclear theory and experiment

N.K. Timofeyuk¹, I.J. Thompson² and J.A. Tostevin¹

¹ Department of Physics, University of Surrey, Guildford GU2 7XH, UK

² LLNL, PO Box 808, Livermore, CA 94551, USA

E-mail: N.Timofeyuk@surrey.ac.uk

Abstract. There exists a class of nuclei that are obtained by adding one nucleon to a loosely-bound nucleon-core system, for example ^{12}Be , ^9C , ^{18}Ne . For such nuclei, one-nucleon overlap integrals that represent single-particle motion can strongly differ from the standard ones due to the correlations between the two nucleons above the core. The possible non-standard overlap behaviour should be included in the interpretation of the experimental data derived from one nucleon removal reactions such as knockout, transfer and breakup, as well as the predictions of low-energy nucleon capture that leads to these nuclei. We investigate the non-standard behaviour within a three-body model and discuss the challenges associated with this problem.

1. Introduction

One of the most productive and perspective ideas in nuclear many-body theory is the concept of independent single-particle motion in the mutually generated mean field. It explains many nuclear observables qualitatively and provides a basis for quantitative descriptions of nuclei within various versions of the shell model. Over the last decade, the experimental study of single-particle motion has shifted towards nuclei near the edge of stability with the emphasis on the occupation probabilities of single-particle orbits as indicators of the evolution of nuclear shell structure near the drip line. These occupancies are usually determined by comparing the measured cross sections of one-nucleon transfer, breakup, knockout and Coulomb dissociation reactions, to those predicted theoretically. In these calculations, the single particle motion is represented by the overlap integral between the many-body wave functions of neighbouring mass A and $A - 1$ nuclei. Most theoretical analyses assume these overlaps can be calculated using potential models that employ standard Woods-Saxon potentials. With these potentials, at radii outside the binding interaction, the overlap integrals achieve their asymptotic form given by an exponential decrease with a decay constant $\kappa = \sqrt{2\mu S_{1N}(A)}/\hbar$ determined by the nucleon separation energy $S_{1N}(A)$, with μ is the $(A - 1)+N$ reduced mass. This region gives important contribution to the amplitudes of one-nucleon removal reactions and is crucial to predict direct nucleon capture reactions relevant to nuclear astrophysics.

It has been shown recently in Ref. [1] that there exist a class of nuclei for which one-nucleon overlaps can reach their asymptotics much later than usual. This class includes the nuclei at the limits of nuclear stability with very similar one- and two-nucleon separation energies, $S_{1N}(A)$ and

$S_{2N}(A)$, both of which are significantly smaller than for stable nuclei. Such nuclei, for example ^{12}Be , ^9C , ^{18}Ne , can be considered as cluster systems of a core and two valence nucleons. The correlations of the two nucleons outside of the nuclear core can lead to non-standard behaviour of the overlap because even when one nucleon is removed far from the center-of-mass of the residual mass $A - 1$ nucleus, it will still be affected by its interaction with the remaining loosely-bound nucleon in $A - 1$.

The possibility for such an effect follows from the Feynman diagram approach in which the asymptotics of the overlap integrals for many-body systems are represented by a sum of different Feynman diagrams. It has been noticed by Blokhintsev [2] that, although in most cases the standard point diagram gives the exponential decrease with the smallest decay constant κ , sometimes other diagrams can give a much slower decrease than that governed by the differences in initial and final binding energies. The Feynman diagram technique, applied in [1] to one-neutron overlaps for core+2N cluster systems, suggests that although the standard term, $\exp(-\kappa r)/r$, dominates at very large r , the contribution $\exp(-\kappa_1 r)/r^{7/2}$ from the generalised triangle diagram, corresponding to the $A \rightarrow (A - 2) + N + N \rightarrow (A - 1) + N$ virtual process, is determined by the decay constant κ_1 that can be larger than κ by only 40%. It means that if the strength of the generalised triangle diagram is large then its contribution can be noticeable for range of r where the standard behaviour $\exp(-\kappa r)/r$ is traditionally assumed to be achieved.

The abnormal asymptotic behaviour was modelled in [1] for the $\langle ^{11}\text{Be} | ^{12}\text{Be} \rangle$ overlap by adding a long-range potential to a local potential model. The resulting overlap was then used to predict longitudinal momentum distributions for one-neutron knockout from ^{12}Be . Comparison of the latter to available experimental data suggests such abnormalities would take place for $n-^{11}\text{Be}$ distances between 5 and 10 fm. However, the contribution from the generalised triangle diagram can be calculated reliably only for $r \gg |\kappa_1 - \kappa|^{-1}$, which for ^{12}Be is $r \gg 2.5$ fm, therefore, to understand the overlap behaviour at $5 \leq r \leq 10$ fm exact dynamical three-body calculations should be carried out.

Here, we calculate one-nucleon overlaps using a three-body core+2N model and compare them to the predictions of the standard potential model (Sec. 2). We discuss effects of non-standard overlap behaviour on nuclear reactions (Sec. 3) and challenge they pose for both theory and experiment (Sec.4).

2. Three-body calculations

We have performed three-body calculations for ^{12}Be ($^{10}\text{Be}+n+n$), ^9C ($^7\text{Be}+p+p$) and ^{18}Ne ($^{16}\text{O}+p+p$) assuming no structure for the ^{10}Be , ^7Be and ^{16}O cores but taking antisymmetrization into account using the Pauli Projection technique [3]. The three-body Schrödinger equation has been solved by expanding the wave functions onto a hyperspherical harmonics basis. The overlap integrals $\langle ^{11}\text{Be} | ^{12}\text{Be} \rangle$, $\langle ^8\text{B} | ^9\text{C} \rangle$ and $\langle ^{17}\text{F} | ^{18}\text{Ne} \rangle$ have been obtained by overlapping the three-body and two-body wave functions. The N -core Woods-Saxon potentials have been fitted to chosen separation energies and the GPT potential [4] has been used for the NN interaction. The Coulomb p -core and pp potentials have been also included for ^9C and ^{18}Ne .

Pseudo ^{12}Be . First of all the convergence of the overlap in the asymptotic region has been tested for a simplified case of ^{12}Be in which the deformation and excitation of the ^{10}Be core have been neglected and the $n-^{11}\text{Be}$ interaction was zero in all partial waves except for $\ell = 0$. This has enabled us to include terms up to $K_{\max} = 120$ in the hyperspherical expansion and to obtain converged values for $\langle ^{11}\text{Be} | ^{12}\text{Be} \rangle$ with high accuracy up to 30 fm. The $n-^{10}\text{Be}$ potential was fitted either to the experimental value of $S_{1N}(^{11}\text{Be})$, 496 keV, or to a much smaller value of 102 keV to check whether the effect from the nn correlations increases with weaker binding. In this particular case, the nn potential was represented by just one Gaussian that gives a scattering length of -20 fm. The three-body energies obtained for ^{12}Be are shown in Table 1. The overlap integrals $\langle ^{11}\text{Be} | ^{12}\text{Be} \rangle$, renormalized to unity, are plotted as ratios to their asymptotics in Fig.1a

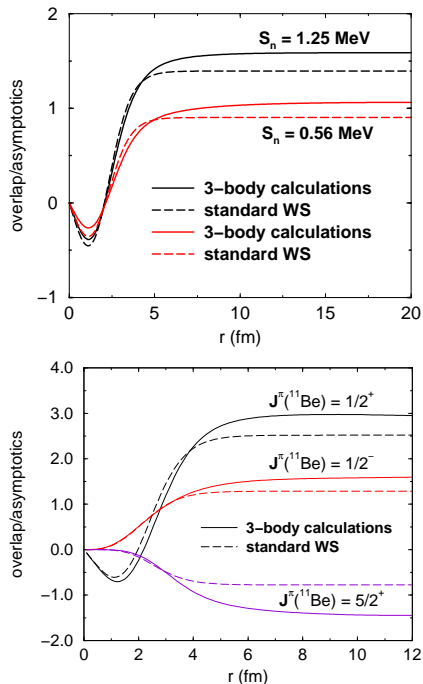


Figure 1. The $\langle {}^{11}\text{Be}|{}^{12}\text{Be}\rangle$ overlaps for pseudo (a) and real (b) ${}^{12}\text{Be}$.

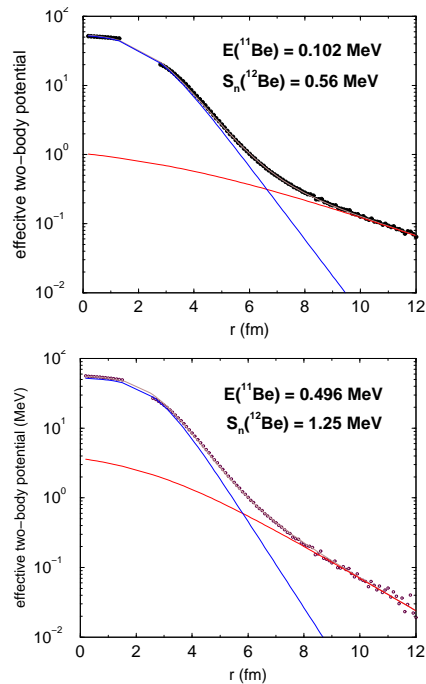


Figure 2. Effective local $n-{}^{11}\text{Be}$ potentials for pseudo ${}^{12}\text{Be}$ fitted by a sum of two Woods-Saxon potentials.

where they are compared to those calculated in a potential model with standard geometry $r_0 = 1.25$ fm and $a = 0.65$ fm. Also, the r.m.s. radii of these overlaps are given in Table 1 in comparison with standard values. The abnormal behaviour is clearly seen for both three-body calculations and, as expected, the abnormalities are stronger for a smaller $S_{1N}({}^{11}\text{Be})$. Fig.2 shows effective local potentials (open circles) obtained by inversion of the two-body Schrödinger equation. They can be fitted by a sum of two Woods-Saxon potentials one of which has unusually large diffuseness (see Table 2).

Realistic ${}^{12}\text{Be}$. To take into account the deformation and the excitation of the ${}^{10}\text{Be}$ core, we have repeated the calculations from [5] for the case EXC1. The model space have been increased up to $K_{\text{max}} = 34$ which has provided a reasonable stability for the overlap $\langle {}^{11}\text{Be}|{}^{12}\text{Be}\rangle$ at $5 \leq r \leq 10$ fm. The abnormal surface behaviour in $\langle {}^{11}\text{Be}|{}^{12}\text{Be}\rangle$ is seen for all three states of the ${}^{11}\text{Be}$ residue (see Fig. 1b) and the effective local $n-{}^{11}\text{Be}$ potentials, the parameters of which are shown in Table 2, have long-range terms although their diffuseness are smaller than in the pseudo ${}^{12}\text{Be}$ case. The abnormalities arise due to the correlations between the two neutrons which are visualised in the plot of the wave function densities in Fig. 3. When the c.m. of two neutrons is far away from the ${}^{10}\text{Be}$ core, the probability that these neutrons are close to each other is high.

Pseudo ${}^9\text{C}$. Our attempts to use the proper spin $J^\pi = \frac{3}{2}^-$ for the ${}^7\text{Be}$ core have been successful only for small model spaces that cannot provide convergence for the overlap in the region of interest. Therefore, we have used $J^\pi = 0^+$ for ${}^7\text{Be}$ and neglected the p - ${}^7\text{Be}$ spin-orbit interaction. This overbinds ${}^9\text{C}$ but enables us to increase the model space up to $K_{\text{max}} = 50$, thus providing high accuracy for $\langle {}^8\text{B}|{}^9\text{C}\rangle$ up to 20 fm. The overlap converges to its asymptotic form slower than in the standard case but not as slow as for ${}^{12}\text{Be}$. The two protons stay close to each other when both are far away from the ${}^7\text{Be}$ core but the weight of this configuration is

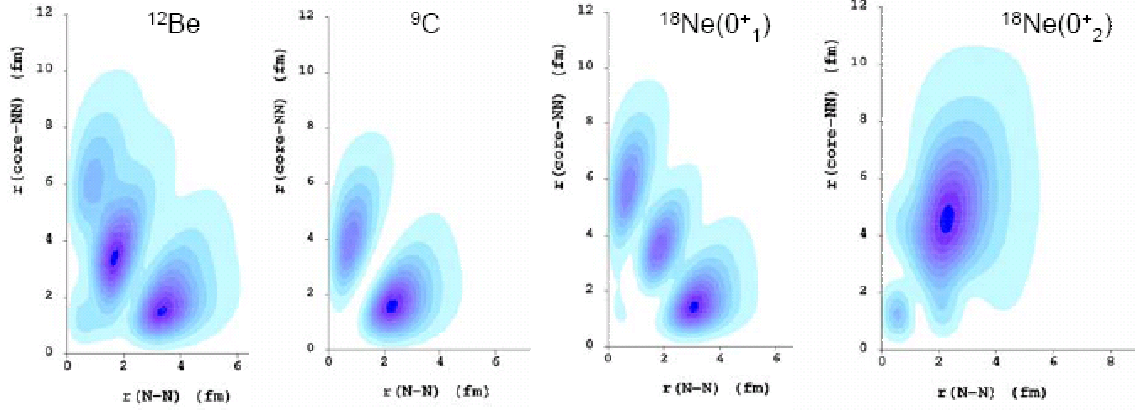


Figure 3. Probability densities of the wave functions obtained in three-body calculations for realistic ^{12}Be , ^{18}Ne and pseudo ^9C .

smaller than in ^{12}Be (see Fig.3).

^{18}Ne . The ^{18}Ne wave functions have been calculated for the ground and first excited 0^+ states in a model space with $K_{\text{max}} = 50$. The pp correlations outside the nuclear interior are clearly seen in the ^{18}Ne wave function and the overlaps differ from the standard ones in the surface region. However, this difference is much smaller than for ^{12}Be , despite the long-range character of the Coulomb force. The three-body dynamics results mainly in an increase of the overlap r.m.s. radius, which is stronger in the s -wave where the centrifugal barrier is absent.

3. Non-standard overlaps in nuclear reactions

Nucleon knockout reactions have recently become a popular tool to determine spectroscopic factors. We have calculated the cross sections and the parallel momentum distributions for

Table 1. One- and two-nucleon separation energies, S_{1N} and S_{2N} (in MeV), and r.m.s. radii (in fm) for overlaps $\langle A-1|A\rangle$ calculated in a three-body model. R.m.s. radii $\langle r^2 \rangle_{st}^{1/2}$ from the fixed standard Woods-Saxon potential are also given.

nucleus A	nucleus $A-1$	$S_{1N}(A-1)$	$S_{1N}(A)$	$S_{2N}(A)$	$\langle r^2 \rangle^{1/2}$	$\langle r^2 \rangle_{st}^{1/2}$
pseudo ^{12}Be	$^{11}\text{Be}(\frac{1}{2}^+)$	0.102	0.56	0.656	7.650	6.983
pseudo ^{12}Be	$^{11}\text{Be}(\frac{1}{2}^+)$	0.496	1.25	1.76	5.807	5.423
real ^{12}Be	$^{11}\text{Be}(\frac{1}{2}^+)$	0.500	3.141	3.641	4.412	4.298
	$^{11}\text{Be}(\frac{1}{2}^-)$	0.180	3.461	3.641	3.588	3.473
	$^{11}\text{Be}(\frac{5}{2}^+)$	-1.09	4.731	3.641	3.738	3.244
pseudo ^9C	^8B	0.149	4.526	4.675	3.175	3.016
$^{18}\text{Ne}(0_1^+)$	$^{17}\text{F}(\frac{5}{2}^+)$	0.603	2.974	3.577	3.602	3.337
	$^{17}\text{F}(\frac{1}{2}^+)$	0.176	3.401	3.577	4.068	3.602
$^{18}\text{Ne}(0_2^+)$	$^{17}\text{F}(\frac{5}{2}^+)$	0.603	2.974	1.141	3.511	3.426
	$^{17}\text{F}(\frac{1}{2}^+)$	0.176	3.401	1.141	4.486	3.947

Table 2. The depth V_i (in MeV), radii r_i and diffusenesses a_i (in fm) of the local effective potentials for the overlap $\langle A-1|A\rangle$ parametrised as a sum of two Woods-Saxon central potentials, $V_0(r) + V_1(r)$, and a spin-orbit potential $V_{so}(r)$.

nucleus A	$A-1$	V_0	r_0	a_0	V_1	r_1	a_1	V_{so}	r_{so}	a_{so}
pseudo ^{12}Be	$^{11}\text{Be}(\frac{1}{2}^+)$	53.5	1.20	0.70	4.8	0.989	1.85			
pseudo ^{12}Be	$^{11}\text{Be}(\frac{1}{2}^+)$	55.9	1.07	0.82	1.5	1.124	3.1			
real ^{12}Be	$^{11}\text{Be}(\frac{1}{2}^+)$	50.0	1.33	0.75	6.9	1.17	1.4			
	$^{11}\text{Be}(\frac{1}{2}^-)$	50.0	0.99	0.79	9.8	1.12	1.55	8.85	1.08	0.80
pseudo ^9C	^8B	54.24	1.10	0.81	2.7	1.2	1.5	8.91	1.10	0.81

$^9\text{Be}(^{12}\text{Be},^{11}\text{Be})\text{X}$ at 90 MeV/nucleon using the $\langle^{11}\text{Be}|^{12}\text{Be}\rangle$ overlap obtained in three-body calculations. The parallel momentum distributions from the three-body $\langle^{11}\text{Be}|^{12}\text{Be}\rangle$ overlap agree with those from the Woods-Saxon potential, provided they have the same r.m.s. radius. The slow convergence of $\langle^{11}\text{Be}|^{12}\text{Be}\rangle$ to its asymptotic form cannot be seen in such an experiment. The momentum distributions depend on the radius of the overlap and thus can be used to determine this if measured with high precision. The cross sections scale almost linearly with the r.m.s. radius of the overlap (see Fig.4) and, therefore, at these energies the effect from surface abnormalities in the $\langle^{11}\text{Be}|^{12}\text{Be}\rangle$ overlap manifests itself only as a change in the overall norm of the calculated cross sections. This will therefore influence spectroscopic factors deduced from comparisons between calculated and measured cross sections.

Transfer reactions are sensitive to the surface part of the overlap and thus could be a good tool to study non-standard single-particle motion in the core+2N cluster systems. A subclass of such reactions, peripheral transfer reactions, determine asymptotic normalization coefficients in the overlap tails thus constraining the overlap r.m.s. radius.

Low-energy direct radiative capture. Proton capture cross sections are often sensitive only to the asymptotic region of the one-nucleon overlap and thus possible abnormal surface behaviour will not influence energy dependence of such reactions. However, the contribution of the surface region to the neutron capture amplitude can be more important. We have performed two-body calculations of the $^{11}\text{Be}(n,\gamma)^{12}\text{Be}$ cross sections using three different $n-^{11}\text{Be}$ interactions: (i) the standard Wood-Saxon potential; (ii) the effective local potential from Table 2 presented by two Woods-Saxon potentials and (iii) a single Woods-Saxon potential that gives exactly the same r.m.s. radius for the $n-^{11}\text{Be}$ wave function as the effective local one. Both

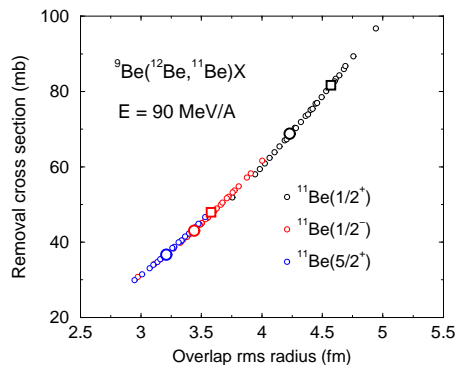


Figure 4. The knockout cross sections populating the final states $^{11}\text{Be}(\frac{1}{2}^+)$ (in black), $^{11}\text{Be}(\frac{1}{2}^-)$ (in red) and $^{11}\text{Be}(\frac{5}{2}^+)$ (in blue) calculated with two-body $n-^{11}\text{Be}$ wave functions calculated for a range of different geometries of the Woods-Saxon potentials (circles). The cross sections corresponding to the standard Woods-Saxon geometry are shown by open circles while those calculated with a sum of two Woods-Saxon potentials from Table 2 are shown by open squares.

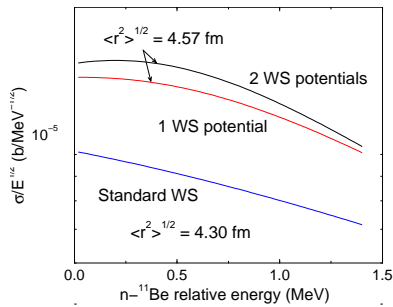


Figure 5. The cross sections for the $^{11}\text{Be}(n,\gamma)^{12}\text{Be}$ reaction divided by square root of the $n-^{11}\text{Be}$ energy calculated with three different $n-^{11}\text{Be}$ potentials. The $\sigma/E^{1/2}$ is shown in logarithmic scale.

the absolute values and the energy dependence of the cross sections, shown in Fig. 5, are very sensitive to the shape of the overlap.

4. Challenges for theory and experiment

The exact dynamical three-body calculations have confirmed the possibility of slower radial convergence of the one-nucleon overlaps to their asymptotic form in core+2N cluster systems due to the strong correlations between the two valence nucleons. This phenomenon has the strongest effect for final core+N systems in relative $l = 0$ states and when the Coulomb interaction is absent. The non-standard behaviour has consequences for the determination of spectroscopic factors from nucleon removal reactions and predictions of neutron capture rates on weakly-bound s -wave nuclei at stellar energies. Therefore, theory must make reliable predictions for non-standard overlaps.

The main challenge for theory is to treat explicitly the three-body dynamics within a many-body object. However, even when internal structure of the core is neglected, the model space, needed to describe the nucleon motion at large distances in coupled-channel hyperspherical calculations, becomes huge. Convergence accelerating methods should be developed to describe properly the core deformation and excitations within the three-body model. Unsolved is the question of how antisymmetrisation influences non-standard behaviour of the overlap. The widely used phenomenological shell model does not generate single-particle wave functions at all so no abnormalities can be seen there. No mean field based theory can reproduce this effect. On the other hand, ab-initio approaches do not yet have sufficient accuracy to study such effects at large distances. For example, keeping in mind that to see unambiguously abnormalities at $5 \leq r \leq 10$ fm in three-body calculations the K_{max} should be at least 30, means that within models of the no-core shell model type at least 30 additional major shells are needed which do not influence the total binding energy. This does not appear feasible at the moment. Three-body dynamics can be included explicitly in microscopic cluster models by hand [6]. However, at present, such models can cope only with the simplest oscillator internal core structure and very simple NN interactions.

Observation of predicted three-body effects in one-nucleon overlaps can be a very difficult task because such effects can be obscured by insufficient knowledge of reaction mechanisms and uncertainties of other inputs to reaction amplitudes. However, unambiguous experimental confirmation either of their presence or absence is very important for our understanding of nuclear dynamics in near-drip line nuclei.

This work was performed under the UK grants EP/C520521/1 and EP/E036627/1 and in the Lawrence Livermore National Laboratory under DoE Contract DE-AC52-07NA27344.

References

- [1] Timofeyuk N K, Blokhintsev L D and Tostevin J A 2003 *Phys. Rev. C* **68** 021601(R)
- [2] Blokhintsev L D 2001 *Bull. Russ. Acad. Sci. Phys.* **65** 77

- [3] Thompson I.J et al 2000 *Phys. Rev. C* **61** 24318
- [4] Gogny D, Pires P and De Tourreil R 1970 *Phys. Lett.* **32** 571
- [5] Nunes F M, Thompson I J and Tostevin J A 2002 *Nucl. Phys. A* **703** 593
- [6] Korennov S and Descouvemont P 2004 *Nucl. Phys. A* 740 249